ARTICLE

Resolving heterogeneity in schizophrenia through a novel systems approach to brain structure: individualized structural covariance network analysis

Zhaowen Liu[1,2,3,29], Lena Palaniyappan[4,5,29], Xinran Wu[6,7], Kai Zhang[8], Jiangnan Du[6,7], Qi Zhao[6,7], Chao Xie[6,7], Yingying Tang[9], Wenjun Su[9], Yarui Wei[10,11,12,13,14,15,16], Kangkang Xue[10,11,12,13,14,15,16], Shaoqiang Han[10,11,12,13,14,15,16], Shih-Jen Tsai[17,18], Ching-Po Lin[7,19,20], Jingliang Cheng[10,11,12,13,14,15,16]✉, Chunbo Li[9], Jijun Wang[9,21,22], Barbara J. Sahakian[6,23], Trevor W. Robbins[6,24], Jie Zhang[6,7]✉ and Jianfeng Feng[6,7,25,26,27,28]✉

Reliable mapping of system-level individual differences is a critical first step toward precision medicine for complex disorders such as schizophrenia. Disrupted structural covariance indicates a system-level brain maturational disruption in schizophrenia. However, most studies examine structural covariance at the group level. This prevents subject-level inferences. Here, we introduce a Network Template Perturbation approach to construct individual differential structural covariance network (IDSCN) using regional gray-matter volume. IDSCN quantifies how structural covariance between two nodes in a patient deviates from the normative covariance in healthy subjects. We analyzed T1 images from 1287 subjects, including 107 first-episode (drug-naive) patients and 71 controls in the discovery datasets and established robustness in 213 first-episode (drug-naive), 294 chronic, 99 clinical high-risk patients, and 494 controls from the replication datasets. Patients with schizophrenia were highly variable in their altered structural covariance edges; the number of altered edges was related to severity of hallucinations. Despite this variability, a subset of covariance edges, including the left hippocampus–bilateral putamen/globus pallidus edges, clustered patients into two distinct subgroups with opposing changes in covariance compared to controls, and significant differences in their anxiety and depression scores. These subgroup differences were stable across all seven datasets with meaningful genetic associations and functional annotation for the affected edges. We conclude that the underlying physiology of affective symptoms in schizophrenia involves the hippocampus and putamen/pallidum, predates disease onset, and is sufficiently consistent to resolve morphological heterogeneity throughout the illness course. The two schizophrenia subgroups identified thus have implications for the nosology and clinical treatment.

Molecular Psychiatry; https://doi.org/10.1038/s41380-021-01229-4

INTRODUCTION

Schizophrenia is considered to be a complex illness with multiple component pathways contributing to the clinical phenotype [1]. Clinical features of this illness may emerge from systems-level disruptions on which the multiple pathways may converge [2, 3]. Network theory allows the study of systems-level interactions.

[1]Psychiatric and Neurodevelopmental Genetics Unit, Center for Genomic Medicine, Massachusetts General Hospital, Boston, MA, USA. [2]Department of Psychiatry, Massachusetts General Hospital, Harvard Medical School, Boston, MA, USA. [3]Stanley Center for Psychiatric Research, Broad Institute of MIT and Harvard, Cambridge, MA, USA. [4]Department of Psychiatry and Robarts Research Institute, University of Western Ontario, London, ON, Canada. [5]Lawson Health Research Institute, London, ON, Canada. [6]Institute of Science and Technology for Brain Inspired Intelligence, Fudan University, Shanghai, P. R. China. [7]Key Laboratory of Computational Neuroscience and Brain Inspired Intelligence, Fudan University, Ministry of Education, Shanghai, P. R. China. [8]School of Computer Science and Technology, East China Normal University, Shanghai, P. R. China. [9]Shanghai Key Laboratory of Psychotic Disorders, Shanghai Mental Health Center, Shanghai Jiao Tong University School of Medicine, Shanghai, P. R. China. [10]Department of Magnetic Resonance Imaging, the First Affiliated Hospital of Zhengzhou University, Zhengzhou, P. R. China. [11]Key Laboratory for Functional Magnetic Resonance Imaging and Molecular Imaging of Henan Province, Zhengzhou, P. R. China. [12]Engineering Technology Research Center for Detection and Application of Brain Function of Henan Province, Zhengzhou, P. R. China. [13]Engineering Research Center of Medical Imaging Intelligent Diagnosis and Treatment of Henan Province, Zhengzhou, P. R. China. [14]Key Laboratory of Magnetic Resonance and Brain Function of Henan Province, Zhengzhou, P. R. China. [15]Key Laboratory of Imaging Intelligence Research Medicine of Henan Province, Zhengzhou, P. R. China. [16]Key Laboratory of Brain Function and Cognitive Magnetic Resonance Imaging of Zhengzhou, Zhengzhou, P. R. China. [17]Institute of Brain Sciences, National Yang-Ming Chiao-Tung University, Taipei, Taiwan. [18]Department of Psychiatry, Taipei Veterans General Hospital, Taipei, Taiwan. [19]Brain Research Center, National Yang-Ming Chiao-Tung University, Taipei, Taiwan. [20]Institute of Neuroscience, National Yang-Ming Chiao-Tung University, Taipei, Taiwan. [21]CAS Center for Excellence in Brain Science and Intelligence Technology (CEBSIT), Chinese Academy of Science, Shanghai, P. R. China. [22]Institute of Psychology and Behavioral Science, Shanghai Jiao Tong University, Shanghai, P. R. China. [23]Department of Psychiatry, School of Clinical Medicine, University of Cambridge, Cambridge, UK. [24]Department of Psychology, Behavioural and Clinical Neuroscience Institute, University of Cambridge, Cambridge, UK. [25]Shanghai Center for Mathematical Sciences, Shanghai, P. R. China. [26]Department of Computer Science, University of Warwick, Coventry, UK. [27]Collaborative Innovation Center for Brain Science, Fudan University, Shanghai, P. R. China. [28]Fudan ISTBI—ZJNU Algorithm Centre for Brain-inspired Intelligence, Zhejiang Normal University, Jinhua, P. R. China. [29]These authors contributed equally: Zhaowen Liu, Lena Palaniyappan ✉email: zhangjie80@fudan.edu.cn ; jffeng@fudan.edu.cn ; cjr.chjl@vip.163.com

Received: 17 March 2021 Revised: 15 June 2021 Accepted: 5 July 2021
Published online: 28 July 2021

Networks based on covariance of brain structure describe shared variation in morphological properties of brain regions across the population, such as gray-matter volume, thickness, surface area, and gyrification [4–8] and demonstrate small world organization [9] and modular structures that closely overlap known functional domains [10]. Structural covariance among brain regions is assumed to reflect anatomical connectivity [11, 12], mutually trophic influences [13], and common experience-driven plasticity [14]. It has been shown to be highly heritable and with significant replicability [4]. Structural covariance relates to IQ at the group level, undergoes significant age-related changes [15], and is informative of disease-related changes that differentiate various brain disorders including schizophrenia [16, 17], autism [18], and Alzheimer's disease [19, 20] from healthy subjects.

Abnormal morphological relationships among cortical structures related to perturbed developmental maturation are considered crucial for understanding the pathophysiology of schizophrenia [4, 6, 21, 22]. However, schizophrenia is a heterogeneous illness with a highly complex genetic architecture [23] and variable phenotypic expressions, thus lacks a unifying neuropathology. Traditional case–control studies are not designed to identify individual differences among patients [24], as the structural covariance network is constructed almost exclusively at the group level, and thus can only be used to identify group-level differences such as abnormalities in frontal-temporal lobe covariance [17]. Mapping individual differences can facilitate finding clinical correlations [25, 26], as well as identifying subgroups of patients with distinctive neuroanatomical patterns.

Recently, normative modeling was introduced as a useful statistical method for mapping the heterogeneity in imaging features at the individual level among patients [27, 28]. For a specific imaging feature, it can provide statistical inferences for the degree to which each individual deviates from the normative pattern, and has been successfully applied to quantify structural heterogeneity in schizophrenia [29, 30], attention-deficit/hyperactivity disorder [31], and autism [32] at the individual level. However, structural covariance networks were traditionally constructed at the group level thus cannot generate a normative distribution, thus normative model cannot be directly employed. Therefore, new approaches for constructing individual level structural covariance networks would hold great promise for uncovering subject-specific deviations in morphological covariance among regions.

To date, such a method has not been well established [5]. Thus, we used a novel approach, Network Template Perturbation, to construct the brain-wide individualized structural covariance network based solely on T1-weighted images, enabling us to explore the heterogeneity of the structural covariance network at the individual level. In line with Marquand et al.'s recent review [28] highlighting the need to (1) exploit normative models in stratification of individual patients and (2) externally validate normative models with symptoms and genotypes, we employ a clustering analysis for stratification (subtyping) and study the symptomatic differences among the identified clusters. We first apply this method to a primary first-episode schizophrenia (FES) dataset (107 drug-naive patients and 71 controls) to test for the presence of distinct subtypes based on deviations in structural covariance. We then studied the stability of the subtypes across illness stages in patients at a chronic (three datasets) and a clinical high-risk (CHR) (one dataset) stage. To establish clinical relevance [28], we contrasted the global symptom profiles of subtypes, without limiting the search to any specific symptoms. Furthermore, we expected the overall degree of normative deviation to relate to hallucination severity based on several prior observations relating altered structural covariance to hallucinations [17, 33, 34]. We also undertook GWAS analysis and large-scale functional annotation analysis for the identified structural covariance edges, to help externally validate their biological meaning [28]. As diagnostic stability is often an issue with first-episode samples, we carefully selected a nosologically distinct group of patients with established schizophrenia, but not schizoaffective disorder or psychotic depression or bipolar disorder. In summary, we expected normative model based structural covariance to yield subtypes that are (1) stable across stages and (2) vary in symptom profile. We did not hypothesize a specific symptom to match a specific covariance profile at the outset.

METHODS AND MATERIALS

Participants

Individuals who participate in this study were recruited from three hospitals including Shanghai Mental Health Center, the First Affiliated Hospital of Zhengzhou University, and Taipei Veteran General Hospital and from another two publicly available datasets, i.e., Center for Biomedical Research Excellence (COBRE) and Mind Clinical Imaging Consortium (MCIC). All patients were identified according to the Diagnosis and Statistic Manual of Mental Disorders, fourth edition (DSM-IV) criteria for schizophrenia by qualified psychiatrists using all available clinical information including a diagnostic interview, clinical case notes, and clinician's observations. The severity of positive and negative symptoms was assessed by trained and experienced psychiatrists using PANSS scoring. Individuals were excluded from the study if they were diagnosed with schizoaffective disorder, mood disorders, other cognitive disorders, epilepsy, had severe physical diseases, alcohol/drug dependence, or been treated with electroconvulsive therapy. The FES patients were defined as having illness duration ≤24 months. All FE schizophrenia patients in this study are drug-naive, and the chronic patients were receiving various antipsychotic medications, see Supplemental Methods for medications details.

We also included CHR subjects who were assessed by a validated Chinese version [35] of the Structured Interview for Prodromal Symptoms [36] and the Scale of Prodromal Symptoms [36], administered by a senior psychiatrist, see Supplemental Methods for details.

Healthy subjects were assessed in accordance with DSM-IV criteria as being free of schizophrenia and other Axis I disorder, and none had neurological diseases, head trauma, substance abuse, suicidal ideation, and MRI contraindications. All participants were between the ages of 14 and 72 years. All studies were approved by the Institutional Review Board of relevant institutes, and all participants provided written informed consent. Data quality was ensured by screening raw data, registration, segmentation, and normalization quality, as well as by excluding left-handers and by matching age and sex. After quality control, 1278 eligible subjects from different institutes completed their T1-weighted image scan and were involved in this study (320 first-episode drug-naive and 294 chronic schizophrenia patients, 99 CHR subjects and 565 matched health controls).

These involve seven datasets as follows: our initial analysis was based on a primary FES dataset with genetic data (107 drug-naive patients and 71 healthy controls) collected from the Shanghai Mental Health Center. Validation dataset #1 consists of 91 subjects (44 drug-naive FES patients, 47 health controls) also from the Shanghai Mental Health Center. Validation dataset #2 contains 224 subjects from the First Affiliated Hospital of Zhengzhou University (166 drug-naive FES patients, 58 health controls). Moreover, three chronic and one CHR datasets were used to explore the stability of our results across different disease stages. Chronic dataset #1 involves 256 subjects from Taipei Veteran General Hospital (124 schizophrenia patients, 132 health controls). Chronic dataset #2 involves 141 subjects from the COBRE (67 patients and 74 controls). Chronic dataset #3 involves 192 subjects from the MCIC (103 patients and 89 controls) [37]. Finally, a CHR dataset consists of 196 subjects from the Shanghai Mental Health Center (99 high-risk individuals, and 97 controls). Additional demographic information and clinical characteristics for all sites are provided in Table 1.

T1 data acquisition and preprocessing

Individuals were all scanned by 3T and 1.5T magnetic resonance scanners: Shanghai Mental Health Center (GE Sigma 3T), the First Affiliated Hospital of Zhengzhou University (GE MR750 3T), National Yang-Ming University in Taiwan (3T Siemens), COBRE (3T Siemens Trio), MIMC (3T Siemens Trio and 1.5T Siemens). The imaging parameters for all datasets are provided in Supplemental Methods. The voxel-based morphometry preprocessing of T1-weighted structural data was carried out using CAT12 (http://dbm.

Table 1. A summary of the demographic information of all seven different datasets used in this study, including one primary FES dataset, two validation FES datasets, three chronic datasets, and one clinical high-risk dataset that were from five different centers/cohorts.

Sites	Number	Age (years)	Sex	Education (years)	TIV	Illness duration	PANSS P	PANSS N	PANSS G
First episode									
Primary FES dataset Shanghai Mental Health Center	Control (71)	25.04 ± 6.31	42/29	12.87 ± 2.86	1453.1 ± 143.3	NA	NA	NA	NA
	Patient (107)	24.05 ± 7.94	65/42	11.90 ± 2.82	1490.6 ± 155.0	27.65 ± 21.61 weeks	20.29 ± 5.79	15.23 ± 6.72	41.52 ± 7.02
Validation dataset #1 Shanghai Mental Health Center	Control (44)	25.24 ± 9.12	28/16	12.68 ± 3.24	1463.7 ± 146.7	NA	NA	NA	NA
	Patient (47)	23.95 ± 5.99	23/24	11.02 ± 2.86	1482.9 ± 147.6	27.41 ± 21.36 weeks	21.93 ± 6.33	14.56 ± 8.14	39.25 ± 7.15
Validation dataset #2 The First Affiliated Hospital of Zhengzhou University	Control (58)	23.58 ± 4.42	33/25	13.02 ± 4.80	1594.6 ± 152.0	NA	NA	NA	NA
	Patient (166)	22.98 ± 8.65	88/78	11.43 ± 2.60	1595.1 ± 149.9	<12 weeks[a]	20.27 ± 4.83	23.46 ± 6.03	±6.51
Chronic									
Chronic dataset #1 Taipei Veteran General Hospital	Control (89)	33.13 ± 12.21	60/29	15.38 ± 2.86	1499.4 ± 136.6	NA	NA	NA	NA
	Patient (103)	34.39 ± 11.03	78/25	12.76 ± 3.40	1428.5 ± 147.1	16.67 ± 10.62 years	9.76 ± 3.08	10.02 ± 4.83	20.83 ± 4.41
Chronic dataset #2 COBRE	Control (74)	35.64 ± 11.69	52/22	14.00 ± 1.78	1512.0 ± 149.5	NA	NA	NA	NA
	Patient (67)	36.74 ± 13.51	44/13	13.20 ± 1.82	1532.6 ± 161.7	14.94 ± 12.00 years	15.03 ± 4.41	14.39 ± 4.40	29.75 ± 7.69
Chronic dataset #3 MCIC	Control (132)	43.97 ± 11.99	57/75	13.99 ± 2.64	1449.4 ± 136.6	NA	NA	NA	NA
	Patient (124)	43.69 ± 11.31	51/73	14.21 ± 3.02	1469.1 ± 146.8	11.05 ± 9.73 years	4.92 ± 2.73[b]	7.37 ± 3.67[b]	NA
Clinical high risk									
Shanghai Mental Health Center	Control (97)	18.79 ± 4.72	52/45	10.81 ± 2.23	1459.9 ± 138.8	NA	NA	NA	NA
	Patient (99)	17.97 ± 4.61	52/47	10.42 ± 2.57	1493.0 ± 148.4	NA	NA	NA	NA

[a]The illness duration of all first-episode patients recruited in The First Affiliated Hospital of Zhengzhou University is within 3 months.
[b]MCIC used Scale for the Assessment of Positive Symptoms (SAPS) and the Scale for the Assessment of Negative Symptoms (SANS) rather than PANSS.

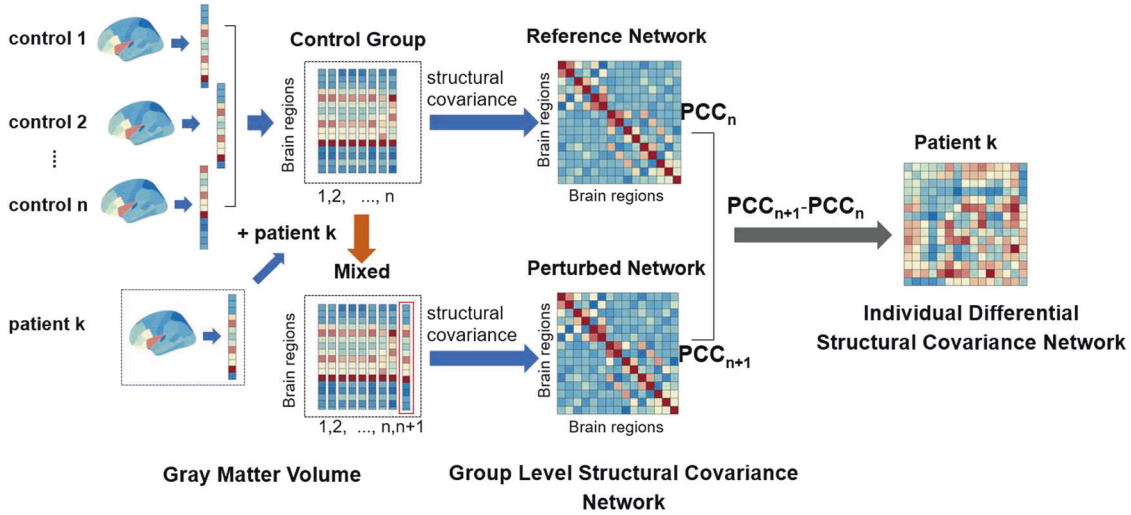

Fig. 1 The workflow for constructing individual differential structural covariance network (IDSCN). A reference structural covariance network was first constructed across all *n* controls, with each edge being the Pearson correlation coefficient between gray-matter volume for each pair of regions (PCC$_n$). Then a new structural covariance network called perturbed network (PCC$_{n+1}$) is constructed by adding patient *k* (*n* controls and 1 patient). IDSCN of the patient *k* was defined as the *Z*-score of the difference between the perturbed network and the reference network base on the *Z*-test described as Eq. 1. *P* value for each edge in IDSCN can be further obtained based on the *Z*-score, indicating the significance of deviation from the control group.

neuro.uni-jena.de/cat), which includes: (1) the T1-weighted images were segmented into GM, white matter (WM), and non-brain voxels (cerebrospinal fluid, skull) using the "new-segment" routine. (2) Population templates (GM, WM) were generated from each of the dataset separately using the DARTEL algorithm [38]. (3) The gray-matter images were aligned to a nonlinear deformation field and normalized to MNI space. (4) The normalized images were all smoothed according to an isotropic Gaussian kernel (full-width at half-maximum = 8 mm). The spatially normalized, smoothed, and Jacobian scaled gray-matter images (voxel size: 1.5 × 1.5 × 1.5 mm, each image had 2,122,945 voxels) were obtained for each subject. The summary statistics for the quality assurance of all the datasets from CAT12 are provided in Supplementary Table S1.

Since voxels with low value of gray matter have variances close to zero and do not apply to the Gaussian error distributions, we masked those low valued voxels with the SPM Masking Toolbox (http://www0.cs.ucl.ac.uk/staff/g.ridgway/masking/) with a software suggested threshold of 0.22 calculated by SPM. As a result, each retained image had a total of 433,584 voxels for further statistical analysis. The automated anatomical labeling2 (AAL2) [39] atlas, which partitioned the brain into 94 regions of interest (47 in each hemisphere), was used to identify the brain regions, see Supplementary Table S2 for details. Genetic data and the corresponding preprocessing pipelines can be seen in Supplemental Methods.

Statistical analysis

Constructing the individual differential structural covariance network (IDSCN). We adapted a recently developed bioinformatics approach that constructed individual-specific gene expression networks [40] to obtain individual structural covariance networks in our case–control study. In each case–control cohort, the mains steps for constructing the IDSCN for each patient with a control group of *n* subjects are as follows (see Fig. 1). First, a reference structural covariance network was constructed across the whole control group (i.e., *n* controls), which was obtained by calculating the correlation (partial Pearson correlation coefficient, PCC) between gray-matter volume for each pair of brain regions with age, gender, education, and total intracranial volume (TIV) being covariates. The reference structural covariance network was represented as PCC$_n$. Then, we added patient *k* to the control group, and used $n+1$ subjects (*n* controls and 1 patient) to construct a new structural covariance network, which we termed as the perturbed network PCC$_{n+1}$. Next, the difference between the perturbed network and the reference network was calculated, i.e., $\Delta PCC_n = PCC_{n+1} - PCC_n$. Finally, as previous work [40] has theoretically confirmed that ΔPCC_n follows a new type of symmetrical distribution called the "volcano distribution," the tail of which is similar to that of the normal distribution, the *Z*-score of ΔPCC_n was calculated based on the *Z*-test (or *U*-test) as follows:

$$Z = \frac{\Delta PCC_n}{\frac{1-PCC_n^2}{n-1}} \quad (1)$$

The IDSCN network for patient *k* was then constructed with the weight of each edge was the *Z*-scores obtained from the *Z*-test described as Eq. 1. The edges in the IDSCN represent how the additional patient changed the covariance of pairs of brain regions in their gray-matter volume against the reference group. We further obtained the *P* value for each edge in the IDSCN network for patient *k* from the *Z*-score.

Finally, we identified edges in each patient's IDSCN that were significantly different from the reference network following Bonferroni correction. Using the above method, we constructed the IDSCN for each patient, each consisting of 4371 edges between the 94 different brain regions in the AAL2 brain atlas (see Supplementary Table S2 for the details of anatomical regions). The edges obtained in each individual network indicate how the covariance between the two connected nodes in a specific patient deviates from the normative covariance observed in unaffected control group, i.e., the weight of subject-specific deviation from the normative covariance of any two nodes.

Subtyping patients using the IDSCN. After constructing IDSCN, we then subgroup the patients based on the selected covariance edges. Specifically, for each edge in the IDSCN, we first counted the number of patients with significant change ($P < 0.05$, Bonferroni corrected) for this edge. We then used the top 20 edges (in terms of the number of affected patients for the edges) as the features to perform k-means clustering analysis (within each dataset), with one minus the Pearson correlation being the distance. We chose the top 20 edges only, as these edges changed in at least 5% of the patients (i.e., four patients). The number of clusters was set between 2 and 5 in the analysis and 100 times of clustering were performed to obtain the final clustering index under each clustering number. The optimal number of clusters had the largest mean silhouette value. After dividing the patients into different subgroups, two-tailed, two-sample *t*-tests were performed to identify which edges differed significantly in different subgroups, with age, gender, education, and TIV as covariates. We also examined if different subgroups of patients showed significant difference in their symptom severity, i.e., the positive and negative syndrome scale (for participants from Shanghai Mental Health Center, the First Affiliated Hospital of Zhengzhou University, COBRE, and Taipei, the symptom scores were measured by positive and negative syndrome scale/PANSS [41]; for MCIC data, the symptom scores were measured by Scale for Assessment of Negative Symptoms/SANS and Scale

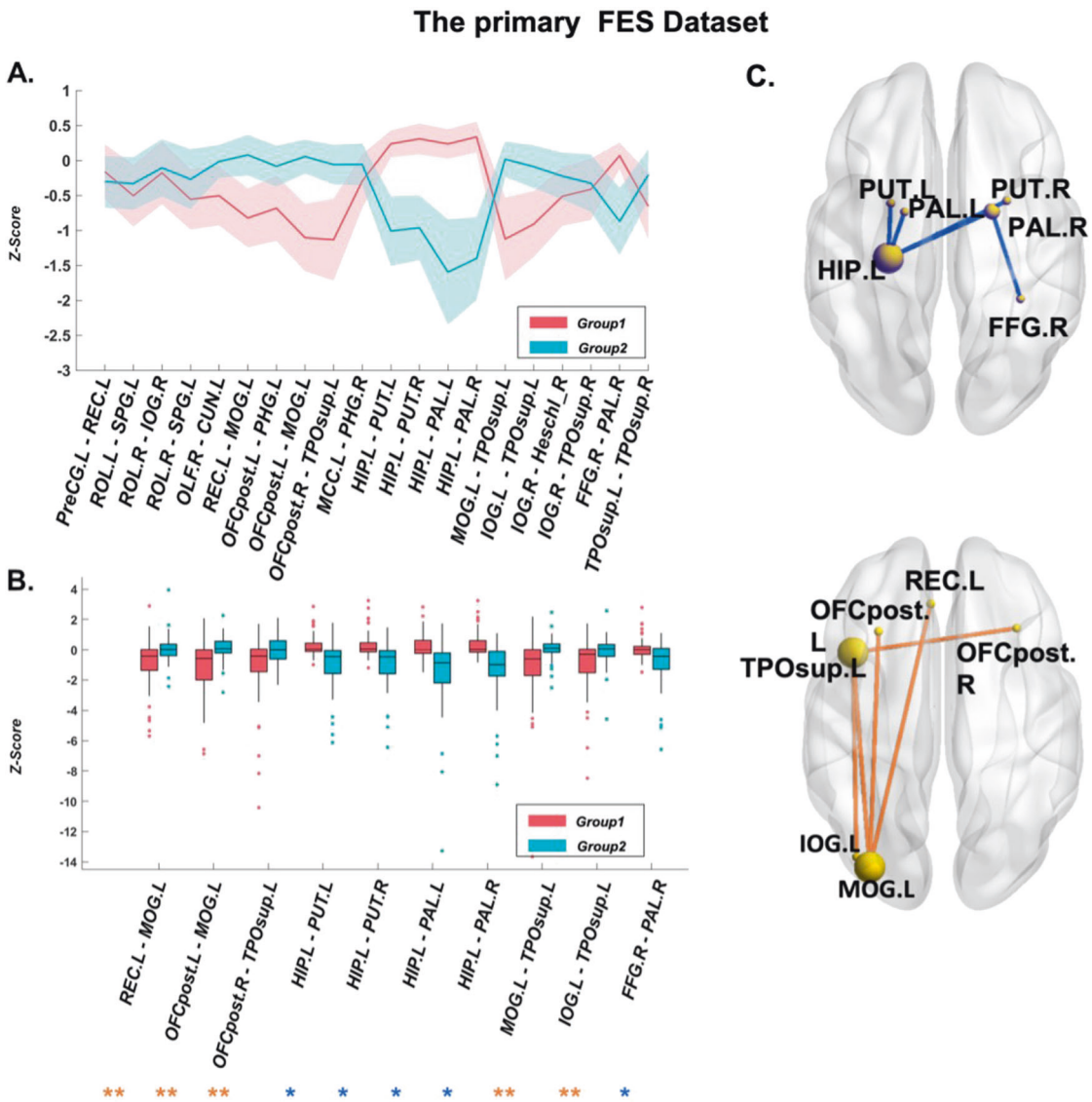

Fig. 2 Division of patients into two different subgroups in the primary FES dataset. A *Z*-score of the top 20 structural covariance edges (with the largest number of patients for which the edge is significantly changed) in the two patient subgroups. **B** The ten edges that show significant difference between the two patient subgroups (group 1 and 2, Bonferroni correction). Blue star and orange double stars indicate two categories of edges with opposite direction of changes in the two patient subgroups. **C** The ten edges in **B** can be classified into two clusters shown in top (blue) and bottom (orange) panel, respectively. Patient group 2 demonstrated lower *Z*-scores than group 1 in the blue edges, while higher *Z*-scores than group 1 in the red edges. Size of the nodes is proportional to their degree.

for Assessment of Positive Symptoms/SAPS [42]) scores, through *t*-tests, with the same covariates. In particular, we studied the association with hallucination severity, a symptom that cuts across all illness stages (CHR, FES to chronic stages) and reported as one of the most prevalent features of this illness.

Validation of the results from the primary dataset. We used the validation approach widely adopted in the literature, i.e., the features identified in the primary dataset (the top 20 edges with the largest number of affected patients) are used in the validation samples to see if these features can produce similar clustering results. To be specific, we check if the clustering results could be validated in another two independent first-episode datasets, and also if the results are consistent across all stages (chronic and CHR) using three chronic schizophrenia datasets and one CHR dataset. Finally, as normative models do not directly indicate whether the deviations have potential clinical utility, we tested external criteria, i.e., the genetic and functional annotation analyses (see Supplemental Methods for details) to parse the causal pathways and phenomenology relevant to the identified structural covariance edges, as suggested by Marquand et al. [28].

RESULTS

A total of 1278 subjects from five different institutes or cohorts (320 first-episode drug-naive and 294 chronic schizophrenia patients, 99 CHR subjects, and 565 matched health controls) were involved after quality control, including one primary FES dataset, two validation FES datasets, three chronic dataset, and one CHR dataset, see Table 1 for detailed demographic information.

Heterogeneity of IDSCNs in first-episode schizophrenia patients

For the primary FES dataset, we constructed the IDSCN for each of the 107 patients using AAL2 atlas that partitioned the brain into 94 different regions. Each edge in IDSCN indicates the level of subject-specific deviation from the normative covariance of the corresponding pair of nodes. We determined the number of edges in each patient's IDSCN that were significantly different from the reference network ($P < 0.05$, Bonferroni corrected for 4317 edges), ranging from 0 to 151 (i.e., 0~3.45% of the total 4317 edges) with a

mean of 17.3 ± 25.9 (SD) edges. Among all 4317 edges, 1367 were found to be significantly changed in at least one of the patients and only 384 out of the 1367 edges were shared by at least two patients, indicating notable heterogeneity of the altered covariance edges among patients. This was supplemented by the low similarity among the IDSCN profile of patients (the between-subjects Pearson correlation among the pairwise *Z*-scores across all the 4317 edges, the mean correlation being 0.0183 ± 0.0689).

Whilst patients did not exhibit notable overlap in their IDSCNs, the regions constituting the fronto-temporo-parietal network were often affected. To prioritize the most affected nodes, we used the 1367 edges that were significantly changed in at least one patient and calculated the degree of each node (the number of edges connecting to it) in the network. The top 10 brain regions with the largest extent of change, including several regions from the fronto-temporo-parietal network [43], are shown in Supplementary Table S3. Furthermore, the higher number of altered edges in their IDSCNs was significantly correlated with higher burden of hallucinations in the PANSS ($r = 0.3166$, $P = 0.0011$).

The relationship between IDSCNs and group-level structural covariance networks

To understand the relationship between the IDSCNs and the traditional group-level structural covariance network, we constructed group-level structural covariance network for control and patient group, respectively, in the primary FES dataset. We defined the group-level difference network dif_{group} as the normalized difference between the two group-level networks. We also calculated the mean of IDSCNs, i.e., $dif_{individual\_mean}$ (detailed in Supplemental Methods). The Pearson correlation between dif_{group} and $dif_{individual\_mean}$ is 0.7496. However, each individual's IDSCN demonstrates a low correlation with the group-level difference network dif_{group} ($r = 0.1901 \pm 0.0946$). These results suggested that the accumulated individual difference contributes the group-level difference, but each individual contributes to the group-level difference in a different way.

Two subgroups of patients with significant difference in depression and anxiety symptoms

We sorted all 4317 edges in the IDSCN according to the number of patients (from large to small) in which the edge is significantly changed. Using the *Z*-score of the top 20 edges (~the top 0.5% of the 4731 edges, which were significantly changed in at least four patients, i.e., about 5% of the patients) as the classifying features, we clustered the patients into two subgroups (k-means clustering, and the silhouette values maximized at two clusters, see Methods). Among the top 20 edges, 10 showed significant differences in their *Z*-score ($P < 0.05$, Bonferroni corrected) between the two subgroups of patients. These ten edges can be separated into two categories with opposite direction of changes among the two subgroups of patients, see Fig. 2B. The first category of edges (five edges, indicated by blue star) connected the left hippocampus with the bilateral putamen and pallidum that showed the most significant difference between the two subgroups of patients (*P* value of the four edges between the left hippocampus and the left and right putamen, and the left and right pallidum being 1.85e–06, 5.93e–07, 1.20e–06, and 3.37e–08, respectively) and another edge connecting the right pallidum with the right fusiform cortex. The second category of edges (five edges, indicated by orange double stars) connected the left

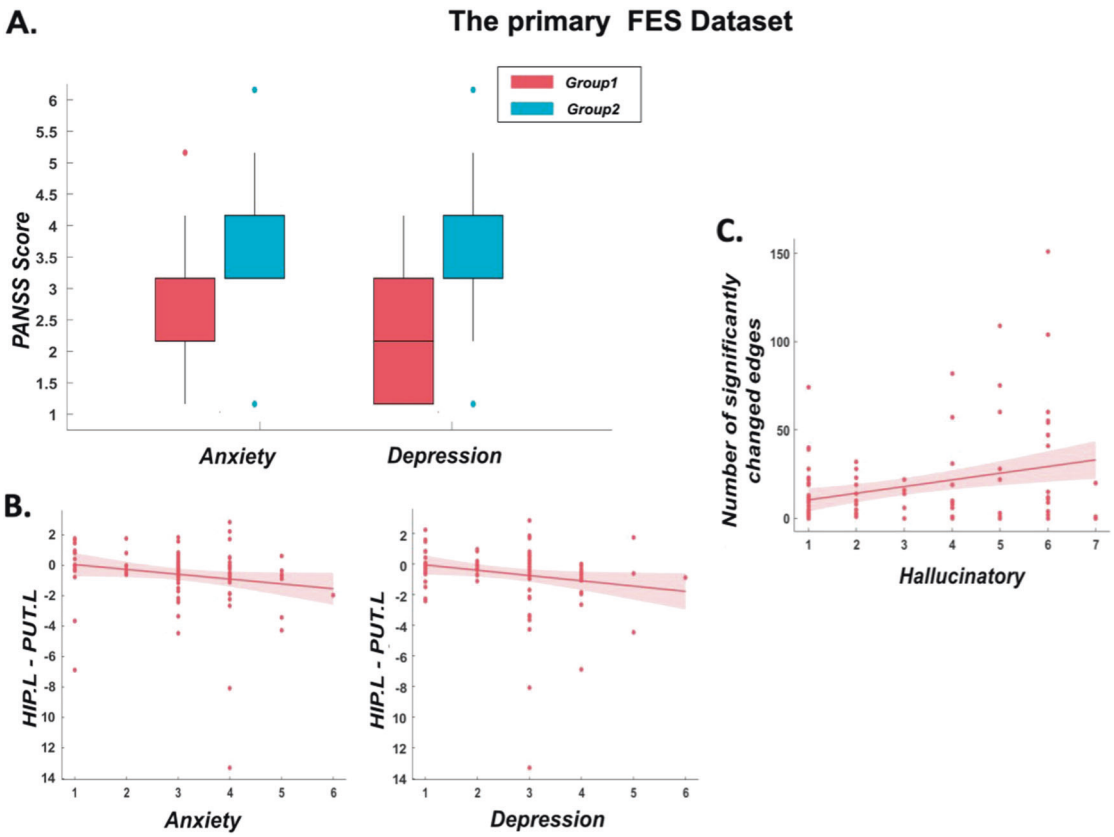

Fig. 3 Significant difference in depression and anxiety score between the two patient subgroups in the primary FES dataset. A The anxiety and depression score of the two patient subgroups, which showed significant difference ($P = 0.0012$ and 1.03e–04, respectively). **B** Scatter plots for the correlation between the individual structural covariance of the left hippocampus and left putamen with the anxiety and depression score ($r = -0.30$, $P = 0.0021$ and $r = -0.24$, $P = 0.014$, respectively). **C** The scatter plot between the number of significantly changed edges in each patient's IDSCN and their hallucination scores ($r = 0.3166$, $P = 0.0011$).

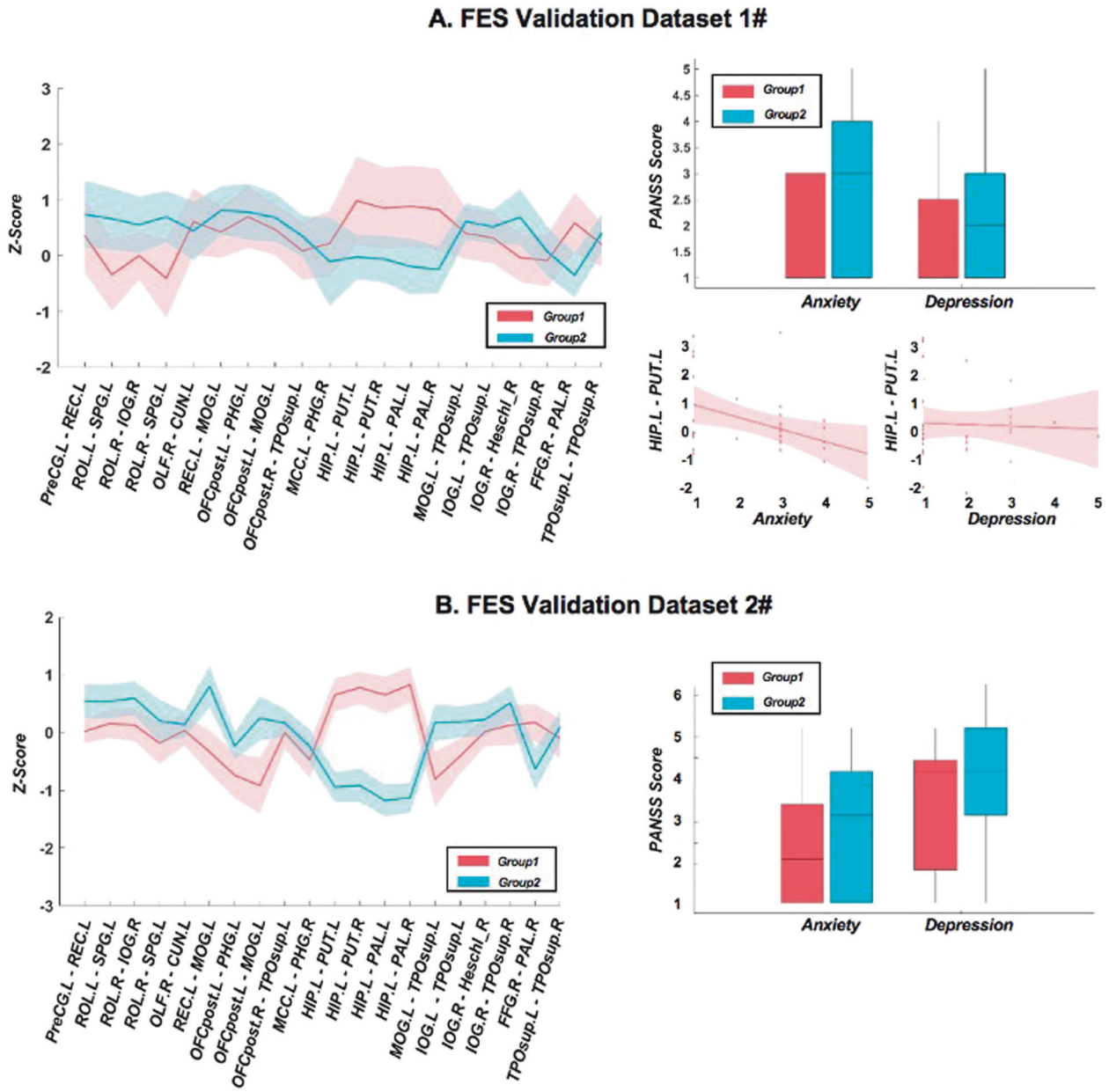

Fig. 4 Validation of the patient subgroup results in two independent FES datasets. A *Z*-scores of the top 20 structural covariance edges in two subgroups, and their clinical scores in the FES validation dataset #1. Patient subgroup 2 was more anxious and depressed than patient group 1, similar to that in the primary FES dataset (although the difference is not statistically significant). The covariance between the left hippocampus and putamen was significantly negatively correlated with the anxiety score ($r = -0.4696$, $P = 0.0367$). **B** *Z*-scores of the top 20 structural covariance edges in two subgroups in FES validation dataset #2. Patient subgroup 2 also shows higher anxiety and depression scores ($P = 0.0122$) than patient group 1, similar to that in the primary FES dataset.

middle occipital gyrus with the left rectus, posterior orbitofrontal cortex, and the superior temporal gyrus, and included edges that connected the left superior temporal cortex with the inferior occipital gyrus and right posterior orbitofrontal cortex.

The two subgroups of patients also exhibited significant differences in their anxiety and depression symptoms on the PANSS general scale ($P = 0.0012$ and 1.03e–04), but did not show significant differences in their sex, age, education, or illness duration ($P = 0.7514$, 0.7309, 0.7410, and 0.2696, respectively). The subgroup of patients with higher *Z*-scores in the first category of edges, i.e., those associated with hippocampal changes, showed less severe burden of depression and anxiety. In addition, we also found that three of the ten edges were significantly correlated with the anxiety or depression score and the *Z*-score for the edge that connected left hippocampus and left putamen was most significantly negatively correlated with both scores ($r = -0.30$, $P = 0.0021$ and $r = -0.24$, $P = 0.0140$, respectively), see Fig. 3 for details.

Validation in two independent first-episode schizophrenia datasets

In order to validate the reliability of the two subgroups of patients identified, we constructed IDSCNs for patients in two FES validation datasets (altogether 213 drug-naive FES patients and 102 controls) and used *Z*-score of the top 20 edges identified in the primary FES dataset to perform the same clustering analysis. All the two validation datasets showed similar differences in pattern between two patient subgroups as that in the primary dataset, see Fig. 4. For the ten edges

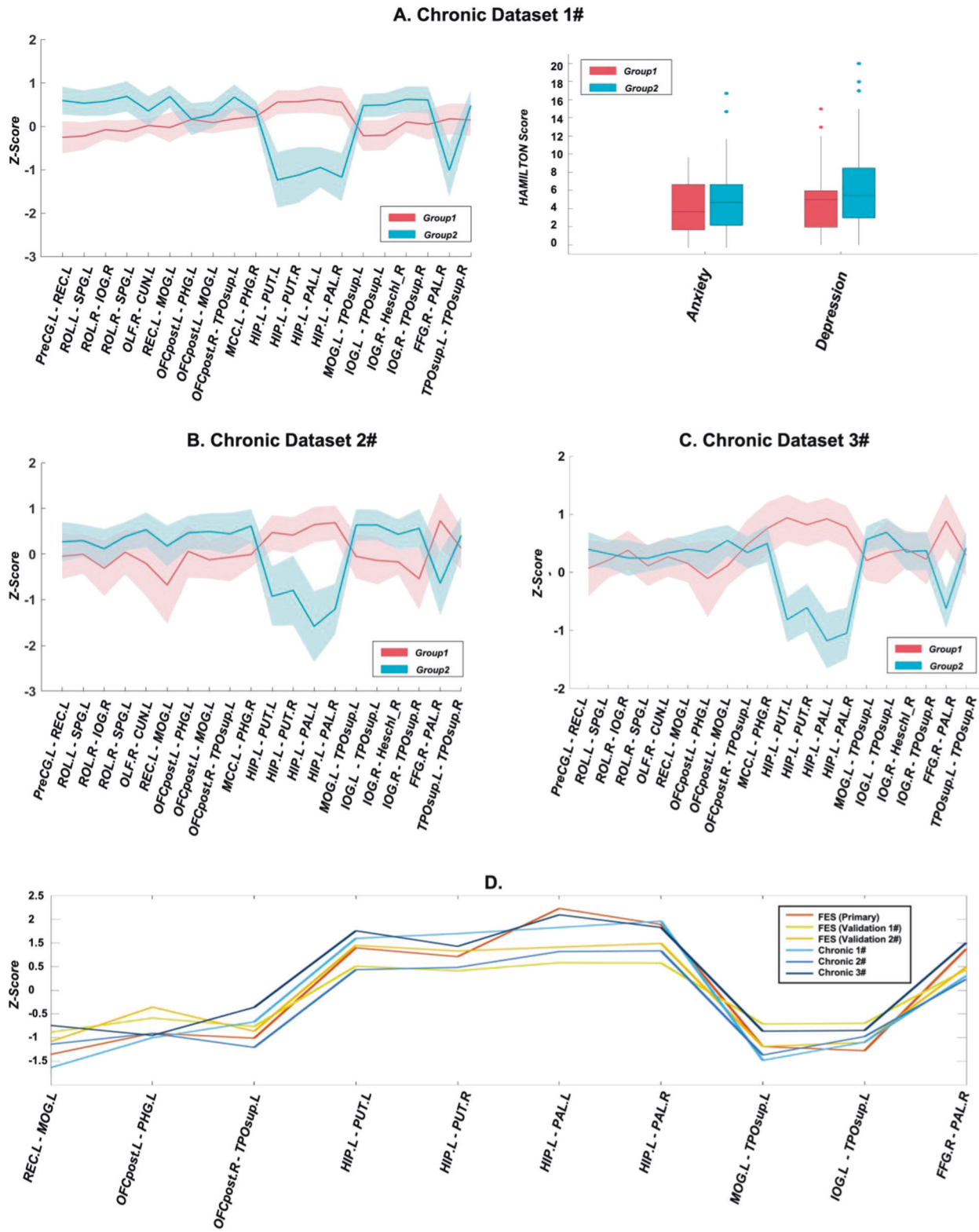

Fig. 5 Patient subgroup results in three chronic schizophrenia datasets. *Z*-scores of the top 20 structural covariance edges in the two patient subgroups for Chronic dataset #1, #2, and #3 are shown in **A**, **B**, and **C**, respectively. For chronic dataset #1, patient subgroup 2 showed higher anxiety and depression scores than group 1, similar to FES datasets. **D** The difference of *Z*-scores between two patient subgroups for the ten edges (showing significant subgroup difference in the primary FES dataset) are plotted for all six schizophrenia datasets. These six datasets demonstrated consistent subgroup differences (pairwise correlation among the six curves being 0.9709 ± 0.0115).

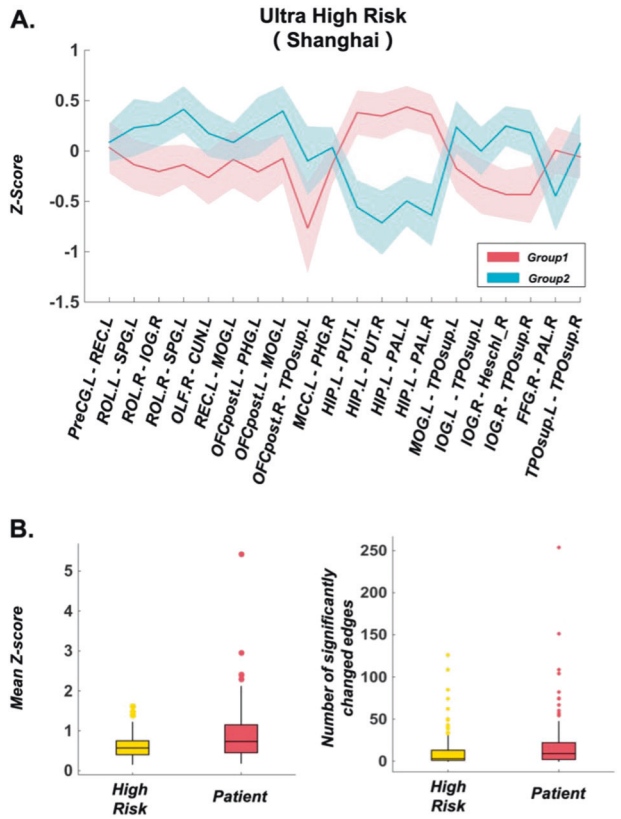

Fig. 6 Patient subgroup results for the clinical high-risk dataset. A The *Z*-scores of the top 20 structural covariance edges in the two subgroups of high-risk individuals. **B** The comparison between the high-risk individuals and FES patients (both collected from the Shanghai Mental Health Center) in their IDSCNs. Left panel: the absolute *Z*-score are averaged over the top 20 edges, for high-risk subjects and the FES patients. The mean absolute *Z*-score is smaller in high-risk individuals than that of FES patients ($P = 1.66e{-}4$, two-tailed, two-sample *t*-test). Right panel: the number of significantly changed edges in IDSCNs for high-risk individuals and FES patients. High-risk individuals show less significant alterations than FES patients ($P = 0.0087$, two-tailed Wilcoxon rank test).

showing significant subgroup difference in FES dataset, five of them (left hippocampus to bilateral putamen/pallidum and right fusiform to pallidum) showed significant difference between two subgroups for both validation datasets (see Supplementary Table S4 for details). Using patients having PANSS scores (32 subjects in Validation dataset #1, 41 subjects in Validation dataset #2), we further replicated that the subgroup differences in the anxiety and depression score in both of the two validation datasets were in the same direction as in the primary FES dataset, with the subgroup difference in depression score being significant for Validation dataset #2 ($P = 0.0122$). The *Z*-score of the edge that connecting left hippocampus and left putamen was consistently negatively correlated with depression and anxiety scores in the two validation datasets and the correlation was significant in the Validation dataset #1 ($r = -0.4696$, $P = 0.0367$, Fig. 4A right panel).

Stability across different stages of schizophrenia

In order to verify the stability of the two subgroups identified in FES patients across different disease stages including CHR and chronic schizophrenia subjects, we constructed IDSCN for another four datasets, including three Chronic Datasets #1-3 (altogether 294 chronic patients and 295 controls), and a CHR Dataset (99 high-risks and 97 controls), and performed k-means clustering using the same 20 edges previously identified in FES. For chronic schizophrenia, all three datasets showed similar subgroup difference pattern as the primary FES dataset in the top 20 edges, see Fig. 5A–C. Importantly, for the ten edges that showed significant subgroup difference in FES dataset, five edges connecting left hippocampus and bilateral putamen/pallidum and right fusiform and pallidum show consistently significant subgroup differences for all three chronic datasets (see Supplementary Table S4 for details). For chronic Dataset #1 with the clinical score, we found that the differences between the two subgroups of patients in anxiety and depression scores were also in the same direction as that validated in the FES dataset, see Fig. 5A. Finally, for the ten edges showing significant subgroup difference in the primary FES dataset, they showed a very similar subgroup difference pattern across all six FES and chronic datasets ($r = 0.9709 \pm 0.0115$, see Fig. 5D).

For CHR individuals, the two subgroups existed and showed similar group difference pre-diagnosis. By k-means clustering using the *Z*-score of the same 20 edges identified from the FES, we found the two subgroups existed prior to diagnosis and these 20 edges showed a similar subgroup difference pattern as those in the FES datasets, see Fig. 6A. The mean absolute *Z*-score averaged over the top 20 edges in high-risk individuals was significantly smaller than that of FES patients from the same center ($P = 1.66e{-}4$, *t*-test, the left panel in Fig. 6), and the number of significantly changed edges in each high-risk individual was significantly less than those in FES patients ($P = 0.0087$, Wilcoxon rank test, right panel in Fig. 6B). These results indicate that the structural covariance network of high-risk individuals showed less normative deviation than FES patients at a whole-brain level.

Functional implications of the covariance edges significantly different between two patient subtypes

To further validate the finding that the subnetwork of IDSCN, showing significant differences between the two subgroups of patients, maybe the underlying neural substrate of affective behavior, we performed a functional annotation analysis for the ten edges showing significant difference between two patient subgroups using the Neurosynth database. Specifically, we used Brain Annotation Toolbox, which transformed the voxel-level functional knowledge from Neurosynth to provide a network-level functional annotation [44]. Functional terms were found to be significantly enriched with BHFDR < 0.05. Among the top 10 terms, 7 were closely related to anxiety/depression (see Supplementary Table S5 for details), which validated our findings that the altered structural covariance correlated with anxiety and depression symptom scores.

Genetic basis for the altered covariance edge by GWAS analysis

To identify the genetic basis of the covariance edge connecting the left hippocampus with the left putamen, which was most significantly correlated with anxiety and depression scores in FES, we used the *Z*-score of the edge in each patient's IDSCN as the phenotype and performed the GWAS analysis. Five SNPs were identified to be significantly associated with the edge, surviving the Bonferroni correction for all the 185,144 SNPs at the $P = 0.05$ level, see Supplementary Fig. S1. The five SNPs related to four genes (POGK, TADA1, SP4, and ZNF778) in chromosomes 1, 7, and 16, respectively. With an FDR threshold <0.1, 28 SNPs in 20 genes were identified to be significantly associated with the edge. Furthermore, we performed a functional enrichment analysis for the 20 genes using the EnrichR [45] website and found that several biological processes related to major histocompatibility complex (MHC) class were significantly enriched, including regulation of the MHC class II biosynthetic process ($P = 3.50e{-}5$) and regulation of the MHC class I biosynthetic process ($P = 0.0070$). HDAC2 and CIITA are two genes involved in these processes. HDAC2 has been shown to play a role in regulating synapse formation and synaptic plasticity in the hippocampus [46].

DISCUSSION

This study used a novel method to construct the brain-wide IDSCN based solely on T1-weighted images. This Network Template Perturbation method enabled exploration of the clinical and genetic correlates of structural covariance, and the identification of covariance-based subgroups in schizophrenia for the first time. We applied the method to a large first-episode schizophrenia dataset and found: (1) individual patients had very low similarity among their IDSCNs at the whole network level, though the overall burden of structural deviance (i.e., the number of significantly altered edges in each patient) reflected the severity of hallucinations. (2) Despite the notable brain-wide heterogeneity, the regions constituting the fronto-temporo-parietal network were often affected [47, 48], indicating shared pathophysiology affecting this network despite the observed heterogeneity. (3) We identified two subgroups of first-episode patients; one with more increased structural covariance for the left hippocampus with the bilateral putamen and pallidum compared to the control group, while the other had reduced covariance and increased depression and anxiety scores compared with the first subgroup; these differences were further validated in two independent FES datasets. This sub-division was stable across different stages of the disorder including CHR, first episode, and the chronic stage. (4) Finally, using a GWAS approach, we identified genes with a role in sensory gating, synapse formation, and synaptic plasticity to play a role in the structural covariance between left hippocampus and the left putamen, providing an important clue to the determinant of structural covariance in schizophrenia.

The results highlight the utility of a normative approach based on individual differences in clustering/subtyping analysis that aims to resolve the clinical and biological heterogeneity of patients. Our method also differed from the approach of Seidlitz et al. to construct individual morphometric similarity networks that focus on estimating the inter-regional correlation of multiple multimodal MRI variables [7]. By contrast, our method estimates inter-regional correlations using a single macro-structural variable, with the edge of each patient's IDSCN representing how far the patient's structural covariance pattern deviated from the healthy reference group, which is consistent with the concept of normative model. The normative models reported to date highlight the presence of structural heterogeneity [29, 30]. However, we went further to leverage this heterogeneity via clustering to identify stable subtypes. Most importantly, our individual-level approach can identify two patient subgroups with opposing patterns in covariance edges (one group higher than controls and the other lower than controls), which would otherwise missed by traditional group-level approaches (i.e., these individual differences will cancel out in group-level approaches). This is consistent with the suggestions that normative modeling permits detection of distinct pattern of abnormality in individuals without requiring a consistent neurobiological signature across all individuals [28].

Our results are broadly consistent with previous studies on brain structural variability and deviance from the expected norm in schizophrenia. For example, Kochunov et.al. calculated the agreement between structural measures from patients and the expected norm from the meta-analytical ranks of schizophrenia-related deficits for each region, demonstrating the prominence of individual deviations in schizophrenia [49]. Brugger et al. employed a meta-analytical approach and reported increased variability in the volume of temporal and subcortical regions in schizophrenia [50]. Using a person-based similarity index that estimates overall group-level covariance across regions, Antoniades et.al. found higher within-group variability among CHR and FEP individuals than healthy controls in cortical thickness, area, and volume [51]. Our approach combines the individual deviation (similar to [49]) and the structural covariance approach (similar to [51]) to estimate variability (as in [50]); thus, we demonstrate that the deviance in the relationships among brain regions is informative of patient-level heterogeneity in schizophrenia.

GWAS analysis of the structural covariance edges between the hippocampus with putamen and pallidum revealed genes implicated in psychiatric disorders. One of the genes, SP4, which is a member of the Sp1 family of transcription factors, has been found expressed abundantly but restrictively in the hippocampus [52]. Hypomorphic SP4 mice display deficits in memory and sensorimotor gating. They also show increased anxiety-like behavior and reduced exploratory responses to the novel environment, which may possibly relate to depression and anxiety symptoms of patients [53]. The gene ZNF778 has also been shown to be related to autism [54]. As the genetic basis of the structural covariance between left hippocampus and the putamen is also implicated in the depression and anxiety-related symptoms, this further supports our conclusions.

The structural covariance between hippocampus and subcortical regions of putamen and pallidum might be a potential underlying neural substrate for differences in the severity of anxiety and depression. From a neuropsychological perspective, this novel functional relationship is consistent with prior preclinical and human studies. The anterior (ventral in rodents) hippocampus has long been associated with affective symptoms of anxiety and depression [55–57] and the hippocampus is intimately associated with prefrontal cortical and ventral reward circuitry in a "limbic-striatal interface" [58]. More recently, it has become clear that the striatum, including the putamen [59, 60], is likely also implicated in the symptoms of depression and anxiety [61–63]. Although there is little evidence to suggest direct anatomical projections of the hippocampus to the putamen, these brain regions are all target regions of midbrain dopaminergic projections; therefore, the covariance in structure may presumably be mediated by dopaminergic influences. We found that the patient subgroup with more severe depression/anxiety symptoms demonstrated less covariance between hippocampus and putamen, which may be related to a disturbance in the midbrain ventral tegmental area that plays a critical role in regulating reward processing and depression [64]. Furthermore, the translational value of early identification of a subgroup of pre-psychotic subjects (CHR) who will later exhibit a higher severity of depression cannot be overstated; depressive symptoms continue to be the most significant predictor of suicide in psychosis and the top treatment priority for patients [65].

In addition, the largest meta-analysis to date of subcortical brain alterations in major depression that was performed by ENIGMA has shown that the volume of the hippocampus was significantly decreased in patients with depression while the volume of putamen was increased in patients although not significantly [66]. Our results are in line with their results as the patients with small *Z*-values for the hippocampus–putamen connection in their IDSCN (which indicated decreased structural covariance between hippocampus and the putamen compared with controls) had higher depression and anxiety scores. It should be noted that patients with schizoaffective disorder were explicitly excluded from the present samples; therefore, our results imply that there are two separable subgroups in schizophrenia: with low and high burden of affective/anxiety symptoms. Thus, the label of non-affective psychosis may indeed be applicable only for a subgroup of individuals with schizophrenia-like psychosis. Such a non-affective group likely has a distinct neural signature (structural covariance) across the various stages of psychosis, influenced by genetic variations. This observation has implications for the etiology, nosology, and treatment of schizophrenia.

To date, most studies have indicated that the morphological changes in schizoaffective illness are closely related to and often indistinguishable from schizophrenia [67, 68]. On this basis, we anticipate that our approach will identify most of the schizoaffective subjects in the schizophrenia + depression/anxiety subgroup.

The patients included in this study did not satisfy schizoaffective criteria; as such, our results indicate that the affective phenomenology in schizophrenia is likely to be mechanistically separable, even if the clinical profile does not warrant the diagnostic label of schizoaffective illness. At present, the treatment of depression is a neglected, unmet need in schizophrenia, though it is associated with high rates of suicide in this illness [69]. Patients often do not explicitly complain feeling low, and psychotic symptoms often trump the overt appearance of depressive features [70]. If our findings are validated independently, this may greatly help in characterizing the mechanism underlying depression in schizophrenia as well as aid in identifying this subgroup that may warrant a different line of management (e.g., antidepressants, cognitive therapy). In this regard, unlike the many existing subgrouping solutions, we offer a clinically actionable MRI-based subgroup approach.

LIMITATIONS

There were several limitations in our study: First, we did not include patients with affective psychosis (e.g., schizoaffective disorder or bipolar disorder with psychosis) for comparison; therefore, the relationship between the schizoaffective disorder and the depressed/anxious subgroup of schizophrenia remains unclear. The presence of two subgroups that differ on depression (affective) burden in a group diagnosed to have non-affective psychosis again highlights the limitations of our current diagnostic system. For schizophrenia patients, we mainly only had their PANSS scores and no other clinical data. We also lacked specific depression scales in CHR subjects. Second, we mainly focused on the results that can be replicated across illness stages. We did not address the stage-specific change (e.g., first-episode to chronic stages) as the site effect cannot be separated from stage effect in this dataset. However, for the CHR and the primary FES datasets that are collected from the same site, we found that the deviation of the covariance edges (compared to the controls) increases from high-risk subjects to first-episode patients. Third, for the genetic analysis, the goal was to identify the mechanistic basis of the structural covariance between left hippocampus with the left putamen, linking pathology to the related symptom [28]. Although genome-wide significant result was found, the sample size was relatively small and further validation from larger datasets should be sought. We also found that the two subgroups we identified had difference in their polygenetic score (PGS) for schizophrenia and MDD. The subgroup with the higher depression and anxiety scores has higher genetic liability for MDD and lower liability for schizophrenia than the subgroup with lower scores. Moreover, the structural covariance between left hippocampus with the left putamen was disrupted in the presence of higher PGS of MDD as well as higher depression and anxiety scores (details in Supplemental Methods). Further testing via large-scale imaging genetic consortia (e.g., ENIGMA) will be essential to replicate our observations in a robust manner. Finally, we constructed the individual structural covariance network based only on gray-matter volume, as the volumetric deficit is one of the most replicated findings in schizophrenia. Our method, however, can be adapted to other structural and morphological measurements, i.e., cortical thickness, surface area, and gyrification.

CONCLUSIONS

Individual structural covariance networks in schizophrenia assist in breaking down the heterogeneity of the disorder. Consistent changes in subcortical (hippocampus–putamen) covariance enable identifying patients with prominent affective symptoms in schizophrenia. Our findings replicated well across independently acquired datasets from different illness stages and provided meaningful leads from the genetic data. Individualized covariance networks identified from single subject scans hold promise in parsing the morphological heterogeneity in psychosis, likely along the lines of depressive symptom burden.

REFERENCES

1. Horváth S, Mirnics K. Schizophrenia as a disorder of molecular pathways. Biol Psychiatry. 2015;77**:** 22–8.
2. Yang GJ, Murray JD, Wang X-J, Glahn DC, Pearlson GD, Repovs G, et al. Functional hierarchy underlies preferential connectivity disturbances in schizophrenia. Proc Natl Acad Sci USA. 2016;113:E219–28.
3. Lo C-YZ, Su T-W, Huang C-C, Hung C-C, Chen W-L, Lan T-H, et al. Randomization and resilience of brain functional networks as systems-level endophenotypes of schizophrenia. Proc Natl Acad Sci USA. 2015;112:9123–8.
4. Alexander-Bloch A, Giedd JN, Bullmore E. Imaging structural co-variance between human brain regions. Nat Rev Neurosci. 2013;14:322–36.
5. Yun J-Y, Boedhoe PS, Vriend C, Jahanshad N, Abe Y, Ameis SH, et al. Brain structural covariance networks in obsessive-compulsive disorder: a graph analysis from the ENIGMA Consortium. Brain. 2020;143:684–700.
6. Palaniyappan L, Park B, Balain V, Dangi R, Liddle P. Abnormalities in structural covariance of cortical gyrification in schizophrenia. Brain Struct Funct. 2015;220:2059–71.
7. Seidlitz J, Váša F, Shinn M, Romero-Garcia R, Whitaker KJ, Vértes PE, et al. Morphometric similarity networks detect microscale cortical organization and predict inter-individual cognitive variation. Neuron. 2018;97:231–47. e237
8. Mechelli A, Friston KJ, Frackowiak RS, Price CJ. Structural covariance in the human cortex. J Neurosci. 2005;25:8303–10.
9. He Y, Chen ZJ, Evans AC. Small-world anatomical networks in the human brain revealed by cortical thickness from MRI. Cereb Cortex. 2007;17:2407–19.
10. Chen ZJ, He Y, Rosa-Neto P, Germann J, Evans AC. Revealing modular architecture of human brain structural networks by using cortical thickness from MRI. Cereb Cortex. 2008;18:2374–81.
11. Lerch JP, Worsley K, Shaw WP, Greenstein DK, Lenroot RK, Giedd J, et al. Mapping anatomical correlations across cerebral cortex (MACACC) using cortical thickness from MRI. Neuroimage. 2006;31:993–1003.
12. Gong G, He Y, Chen ZJ, Evans AC. Convergence and divergence of thickness correlations with diffusion connections across the human cerebral cortex. Neuroimage. 2012;59:1239–48.
13. Pezawas L, Verchinski BA, Mattay VS, Callicott JH, Kolachana BS, Straub RE, et al. The brain-derived neurotrophic factor val66met polymorphism and variation in human cortical morphology. J Neurosci. 2004;24:10099–102.
14. Draganski B, Gaser C, Busch V, Schuierer G, Bogdahn U, May A. Neuroplasticity: changes in grey matter induced by training. Nature. 2004;427:311–2.
15. Zielinski BA, Gennatas ED, Zhou J, Seeley WW. Network-level structural covariance in the developing brain. Proc Natl Acad Sci USA. 2010;107:18191–6.
16. Mitelman SA, Buchsbaum MS, Brickman AM, Shihabuddin L. Cortical intercorrelations of frontal area volumes in schizophrenia. Neuroimage. 2005;27:753–70.
17. Modinos G, Vercammen A, Mechelli A, Knegtering H, McGuire PK, Aleman A. Structural covariance in the hallucinating brain: a voxel-based morphometry study. J Psychiatry Neurosci. 2009;34:465.
18. McAlonan GM, Cheung V, Cheung C, Suckling J, Lam GY, Tai K, et al. Mapping the brain in autism. A voxel-based MRI study of volumetric differences and intercorrelations in autism. Brain. 2005;128:268–76.
19. He Y, Chen Z, Evans A. Structural insights into aberrant topological patterns of large-scale cortical networks in Alzheimer's disease. J Neurosci. 2008;28:4756–66.
20. Seeley WW, Crawford RK, Zhou J, Miller BL, Greicius MD. Neurodegenerative diseases target large-scale human brain networks. Neuron. 2009;62:42–52.
21. Moberget T, Doan N, Alnæs D, Kaufmann T, Córdova-Palomera A, Lagerberg T, et al. Cerebellar volume and cerebellocerebral structural covariance in schizophrenia: a multisite mega-analysis of 983 patients and 1349 healthy controls. Mol Psychiatry. 2018;23:1512–20.
22. Evans AC. Networks of anatomical covariance. Neuroimage. 2013;80:489–504.
23. Rodriguez-Murillo L, Gogos JA, Karayiorgou M. The genetic architecture of schizophrenia: new mutations and emerging paradigms. Annu Rev Med. 2012;63:63–80.
24. Catts VS, Fung SJ, Long LE, Joshi D, Vercammen A, Allen KM, et al. Rethinking schizophrenia in the context of normal neurodevelopment. Front Cell Neurosci. 2013;7:60.
25. Ajnakina O, Das T, Lally J, Di Forti M, Pariante CM, Marques TR, et al. Structural covariance of cortical gyrification at illness onset in treatment resistance: a longitudinal study of first-episode psychoses. Schizophr Bull. 2021;sbab035.

26. Das T, Borgwardt S, Hauke DJ, Harrisberger F, Lang UE, Riecher-Rossler A, et al. Disorganized gyrification network properties during the transition to psychosis. JAMA Psychiatry. 2018;75:613–22.
27. Marquand AF, Rezek I, Buitelaar J, Beckmann CF. Understanding heterogeneity in clinical cohorts using normative models: beyond case-control studies. Biol Psychiatry. 2016;80:552–61.
28. Marquand AF, Kia SM, Zabihi M, Wolfers T, Buitelaar JK, Beckmann CF. Conceptualizing mental disorders as deviations from normative functioning. Mol Psychiatry. 2019;24:1415–24.
29. Wolfers T, Doan NT, Kaufmann T, Alnæs D, Moberget T, Agartz I, et al. Mapping the heterogeneous phenotype of schizophrenia and bipolar disorder using normative models. JAMA Psychiatry. 2018;75:1146–55.
30. Lv J, Di Biase M, Cash RF, Cocchi L, Cropley VL, Klauser P, et al. Individual deviations from normative models of brain structure in a large cross-sectional schizophrenia cohort. Mol Psychiatry. 2020. https://doi.org/10.1038/s41380-020-00882-5.
31. Wolfers T, Beckmann CF, Hoogman M, Buitelaar JK, Franke B, Marquand AF. Individual differences v. the average patient: mapping the heterogeneity in ADHD using normative models. Psychol Med. 2020;50:314–23.
32. Zabihi M, Oldehinkel M, Wolfers T, Frouin V, Goyard D, Loth E, et al. Dissecting the heterogeneous cortical anatomy of autism spectrum disorder using normative models. Biol Psychiatry Cogn Neurosci Neuroimaging. 2019;4:567–78.
33. Heinze K, Reniers RL, Nelson B, Yung AR, Lin A, Harrison BJ, et al. Discrete alterations of brain network structural covariance in individuals at ultra-high risk for psychosis. Biol Psychiatry. 2015;77:989–96.
34. Zhang X, Liu W, Guo F, Li C, Wang X, Wang H, et al. Disrupted structural covariance network in first episode schizophrenia patients: evidence from a large sample MRI-based morphometric study. Schizophr Res. 2020;224:24–32.
35. Ivarsson T, Larsson B. The Obsessive-Compulsive Symptom (OCS) scale of the Child Behavior Checklist: a comparison between Swedish children with Obsessive-Compulsive Disorder from a specialized unit, regular outpatients and a school sample. J Anxiety Disord. 2008;22:1172–9.
36. Kang S, Hong S-I, Lee J, Peyton L, Baker M, Choi S, et al. Activation of astrocytes in the dorsomedial striatum facilitates transition from habitual to goal-directed reward-seeking behavior. Biol Psychiatry. 2020;88:797–808.
37. Gollub RL, Shoemaker JM, King MD, White T, Ehrlich S, Sponheim SR, et al. The MCIC collection: a shared repository of multi-modal, multi-site brain image data from a clinical investigation of schizophrenia. Neuroinformatics. 2013;11:367–88.
38. Ashburner J. A fast diffeomorphic image registration algorithm. Neuroimage. 2007;38:95–113.
39. Rolls ET, Joliot M, Tzourio-Mazoyer N. Implementation of a new parcellation of the orbitofrontal cortex in the automated anatomical labeling atlas. Neuroimage. 2015;122:1–5.
40. Liu X, Wang Y, Ji H, Aihara K, Chen L. Personalized characterization of diseases using sample-specific networks. Nucleic Acids Res. 2016;44:e164.
41. Kay SR, Fiszbein A, Opler LA. The positive and negative syndrome scale (PANSS) for schizophrenia. Schizophr Bull. 1987;13:261–76.
42. Andreasen NC. Methods for assessing positive and negative symptoms. Mod Probl Pharmacopsychiatry. 1990;24:73–88.
43. Brent BK, Seidman LJ, Thermenos HW, Holt DJ, Keshavan MS. Self-disturbances as a possible premorbid indicator of schizophrenia risk: a neurodevelopmental perspective. Schizophr Res. 2014;152:73–80.
44. Liu Z, Rolls ET, Liu Z, Zhang K, Yang M, Du J, et al. Brain annotation toolbox: exploring the functional and genetic associations of neuroimaging results. Bioinformatics. 2019;35:3771–8.
45. Kuleshov MV, Jones MR, Rouillard AD, Fernandez NF, Duan Q, Wang Z, et al. Enrichr: a comprehensive gene set enrichment analysis web server 2016 update. Nucleic Acids Res. 2016;44:W90–7.
46. Guan J-S, Haggarty SJ, Giacometti E, Dannenberg J-H, Joseph N, Gao J, et al. HDAC2 negatively regulates memory formation and synaptic plasticity. Nature. 2009;459:55–60.
47. Spreng RN, DuPre E, Ji JL, Yang G, Diehl C, Murray JD, et al. Structural covariance reveals alterations in control and salience network integrity in chronic schizophrenia. Cereb Cortex. 2019;29:5269–84.
48. Antonova E, Sharma T, Morris R, Kumari V. The relationship between brain structure and neurocognition in schizophrenia: a selective review. Schizophr Res. 2004;70:117–45.
49. Kochunov P, Fan F, Ryan MC, Hatch KS, Tan S, Jahanshad N, et al. Translating ENIGMA schizophrenia findings using the regional vulnerability index: association with cognition, symptoms, and disease trajectory. Hum Brain Mapp. 2020. https://doi.org/10.1002/hbm.25045.
50. Brugger SP, Howes OD. Heterogeneity and homogeneity of regional brain structure in schizophrenia: a meta-analysis. JAMA Psychiatry. 2017;74:1104–11.
51. Antoniades M, Haas SS, Modabbernia A, Bykowsky O, Frangou S, Borgwardt S, et al. Personalized estimates of brain structural variability in individuals with early psychosis. Schizophr Bull. 2021;sbab005.
52. Zhou X, Qyang Y, Kelsoe J, Masliah E, Geyer M. Impaired postnatal development of hippocampal dentate gyrus in Sp4 null mutant mice. Genes Brain Behav. 2007;6:269–76.
53. Zhou X, Long J, Geyer M, Masliah E, Kelsoe J, Wynshaw-Boris A, et al. Reduced expression of the Sp4 gene in mice causes deficits in sensorimotor gating and memory associated with hippocampal vacuolization. Mol Psychiatry. 2005;10:393–406.
54. Willemsen MH, Fernandez BA, Bacino CA, Gerkes E, de Brouwer AP, Pfundt R, et al. Identification of ANKRD11 and ZNF778 as candidate genes for autism and variable cognitive impairment in the novel 16q24. 3 microdeletion syndrome. Eur J Hum Genet. 2010;18:429–35.
55. Gray JA. The neuropsychology of anxiety. Issues Ment Health Nurs. 1985;7:201–28.
56. Roddy DW, Farrell C, Doolin K, Roman E, Tozzi L, Frodl T, et al. The hippocampus in depression: more than the sum of its parts? Advanced hippocampal substructure segmentation in depression. Biol Psychiatry. 2019;85:487–97.
57. Sheline YI, Liston C, McEwen BS. Parsing the hippocampus in depression: chronic stress, hippocampal volume, and major depressive disorder. Biol Psychiatry. 2019;85:436–8.
58. Groenewegen HJ, Trimble M. The ventral striatum as an interface between the limbic and motor systems. CNS Spectr. 2007;12:887–92.
59. Qiao J, Li A, Cao C, Wang Z, Sun J, Xu G. Aberrant functional network connectivity as a biomarker of generalized anxiety disorder. Front Hum Neurosci. 2017;11:626.
60. Wang X, Li J, Yuan Y, Wang M, Ding J, Zhang J, et al. Altered putamen functional connectivity is associated with anxiety disorder in Parkinson's disease. Oncotarget. 2017;8:81377.
61. Price JL, Drevets WC. Neural circuits underlying the pathophysiology of mood disorders. Trends Cogn Sci. 2012;16:61–71.
62. Root DH, Melendez RI, Zaborszky L, Napier TC. The ventral pallidum: subregion-specific functional anatomy and roles in motivated behaviors. Prog Neurobiol. 2015;130:29–70.
63. Lago T, Davis A, Grillon C, Ernst M. Striatum on the anxiety map: small detours into adolescence. Brain Res. 2017;1654:177–84.
64. Tye KM, Mirzabekov JJ, Warden MR, Ferenczi EA, Tsai H-C, Finkelstein J, et al. Dopamine neurons modulate neural encoding and expression of depression-related behaviour. Nature. 2013;493:537–41.
65. Shen C, Luo Q, Chamberlain SR, Morgan S, Romero-Garcia R, Du J, et al. What is the link between attention-deficit/hyperactivity disorder and sleep disturbance? A multimodal examination of longitudinal relationships and brain structure using large-scale population-based cohorts. Biol Psychiatry. 2020;88:459–69.
66. Schmaal L, Veltman DJ, van Erp TG, Sämann P, Frodl T, Jahanshad N, et al. Subcortical brain alterations in major depressive disorder: findings from the ENIGMA Major Depressive Disorder working group. Mol Psychiatry. 2016;21:806–12.
67. Madre M, Canales-Rodríguez EJ, Ortiz-Gil J, Murru A, Torrent C, Bramon E, et al. Neuropsychological and neuroimaging underpinnings of schizoaffective disorder: a systematic review. Acta Psychiatr Scandinavica. 2016;134:16–30.
68. Arnold SJ, Ivleva EI, Gopal TA, Reddy AP, Jeon-Slaughter H, Sacco CB, et al. Hippocampal volume is reduced in schizophrenia and schizoaffective disorder but not in psychotic bipolar I disorder demonstrated by both manual tracing and automated parcellation (FreeSurfer). Schizophr Bull. 2015;41:233–49.
69. Gregory A, Mallikarjun P, Upthegrove R. Treatment of depression in schizophrenia: systematic review and meta-analysis. Br J Psychiatry. 2017;211:198–204.
70. Upthegrove R, Marwaha S, Birchwood M. Depression and schizophrenia: cause, consequence, or trans-diagnostic issue? Schizophr Bull. 2017;43:240–4.

ACKNOWLEDGEMENTS

The neuroimaging and genetic data used here are from ZIB Consortium. JZ was supported by Shanghai Municipal Science and Technology Major Project (No.2018SHZDZX01) and ZJLab, 2016YFC0906402 and National Natural Science Foundation of China (NSFC 61973086). JF was supported by the 111 Project (No. B18015), the key project of Shanghai Science and Technology (No. 16JC1420402), National Key R&D Program of China (No. 2018YFC1312900), and National Natural Science Foundation of China (NSFC 91630314). LP acknowledges salary support from the Tanna Schulich Chair of Neuroscience and Mental Health. JW was supported by National Natural Science Foundation of China (81971251), Science and Technology Commission of Shanghai Municipality (No. 19411969100, 19410710800), and Clinical Research Center at Shanghai Mental Health Center (CRC2018ZD01, CRC2018ZD04, CRC2018YB01, and CRC2019ZD02).

COMPETING INTERESTS

LP reports personal fees from Janssen Canada, Otsuka Canada, SPMM Course Limited, UK, Canadian Psychiatric Association; book royalties from Oxford University Press; investigator-initiated educational grants from Janssen Canada, Sunovion, and Otsuka

Canada outside the submitted work. All other authors report no biomedical financial interests or potential conflicts of interest. None of the above-listed companies or funding agencies have had any influence on the content of this article.

ADDITIONAL INFORMATION

Supplementary information The online version contains supplementary material available at https://doi.org/10.1038/s41380-021-01229-4.

Correspondence and requests for materials should be addressed to J.Z., J.F., or J.C.